Electronic Structure and Orbital Interactions in Linear PtCO

Harold Basch* and Drora Cohen

Contribution from the Department of Chemistry, Bar-Ilan University, Ramat Gan, Israel 52100.
Received November 12, 1982

Abstract: The electronic and geometric structural properties of linear PtCO have been investigated by using an ab initio *l*-dependent relativistic effective core potential for Pt within the framework of the multiconfiguration self-consistent field and configuration interaction methods. The energy ordering of electronic states is found to be $^1\Sigma^+ < (^3\Sigma^+, ^3\Delta) < ^3\Pi$, where $^1\Sigma^+$ correlates with Pt $5d^{10}(^1S)$ and the triplet states arise from the Pt $5d^96s^1(^3D)$ atomic multiplet in the dissociated limits. Upon complexation with a Pt atom the loss of C=O antibonding character in the carbon lone-pair orbital dominates the decrease in π bonding due to the Pt($5d_\pi$)–CO(π^*) interaction. Charge transfer between the Pt and CO fragments is dominated by the CO→Pt σ dative bond at larger Pt–CO distances and by Pt→CO π-back-bonding at shorter bond lengths. The extra stability and shorter equilibrium Pt–CO bond distance of the ground $^1\Sigma^+$ state is due to nonoccupancy of the strongly antibonding σ orbital which in the triplet states has mainly Pt 6s character. This, in turn, allows a closer approach of CO to Pt and enhanced π bonding. Both $^3\Sigma$ and $^3\Delta$ are calculated to be bound on the SCF level while $^3\Pi$ has a repulsive Pt–CO energy interaction curve even with configuration interaction, apparently due to reduced π bonding in its primary electronic configuration. The $^1\Sigma^+$ state in its equilibrium geometry has a Pt atom configuration that is much closer to $5d^96s^1$ than to $5d^{10}$ while the 5d orbital population in the $^3\Delta$ state is close to 8 e.

Current interest in small transition-metal cluster complexes has been heightened by the proposed triangular relationship between isolated metal clusters, polynuclear metal complexes, and metal surface chemisorption.[1-3] The pervasiveness of CO as a ligand and surface adsorbant has naturally led to concentrated activity in metal–CO bond studies. There have recently been a number of theoretical studies of the electronic structure and bonding in the bare NiCO fragment, where interest has been focused on the nature of the electronic ground state and the role of metal–CO π bonding.[4-7] These studies have been hampered by the well-known differential correlation energy problems[8,9] associated with the $3d^{10}(^1S)$, $3d^94s^1(^3D)$, and $3d^84s^2(^3F)$ electronic states of the nickel atom: a proper description of which could be crucial to even the correct theoretical identification of the NiCO electronic ground state.

In the use of NiCO, for example, as a model for larger metal cluster–ligand or metal–adsorbate systems a complication arises from the dominance of the metal 4s orbital in the σ-bond interaction in the model system. However, as shown, for example, in the NiC_2H_4 and $Ni_2C_2H_4$ study,[10] as the metal part of the system increases in size the metal 3d orbital is found to play an increased bonding role. The usefulness of the small model system in this specific case is, therefore, called into question.

The bare PtCO fragment has also been identified in low-temperature matrix isolation experiments.[11] Recent studies have shown that with use of an *l*-averaged relativistic effective core potential (RECP) the differential correlation energy errors in the calculated (*J*-averaged) ^1S, ^3D, and ^3F state multiplet splittings are much smaller in Pt than in Ni.[12] This, of course, neglects spin–orbit splitting effects. Furthermore, in both PtH and Pt_2 the metal 5d orbital has been found to be an important contributor to σ bonding,[13] and this could very well be true also for PtCO. This situation should simplify comparisons with larger metal–

Table I. Parameters for the Platinum Atom Effective Core Potential[a]

k	n_{kl}	α_{kl}	d_{kl}
		$L = 4$	
1	2	1.399 65	−3.478 381
2	2	3.811 13	−20.744 16
3	2	11.899 4	−94.118 43
4	2	39.919 7	−210.069 8
5	1	115.953	−44.015 44
6	0	0.327 480	−0.145 738 7
		$l = 3$	
1	2	1.142 12	2.153 581
2	2	3.810 07	16.668 90
3	2	11.740 6	69.691 64
4	2	165.489	1007.254
5	1	31.388 9	50.852 04
6	0	382.602	3.860 396
		$l = 2$	
1	2	0.440 885	−0.622 080 8
2	2	5.159 34	23.846 50
3	2	13.471 6	98.118 60
4	2	41.642 9	471.412 9
5	2	143.946	1612.478
6	1	391.394	156.587 0
7	0	1.150 28	2.993 334
		$l = 1$	
1	2	0.543 490	3.056 435
2	2	1.606 90	16.690 22
3	2	4.174 50	51.252 60
4	2	9.564 80	95.837 61
5	2	59.511 0	−586.147 4
6	1	46.998 0	116.677 4
7	0	1.656 30	1.740 250
		$l = 0$	
1	2	0.512 407	1.861 196
2	2	1.442 79	14.218 69
3	2	3.915 19	51.410 84
4	2	9.825 90	73.136 34
5	2	52.074 8	−242.072 1
6	1	35.672 3	82.636 08
7	0	18.341 3	0.652 235 9

[a] The total potential is written as[15] $U^c(r) = U^c{}_L(r) + \Sigma_{l=0}^{L-1} \Sigma_{m_l=-l}^{l} |lm_l> [U^c{}_l(r) - U^c{}_L(r)] <lm_l|$, where the fitted parameters belong to $r^2[U^c{}_l(r) - (N_c/r)] = \Sigma_k d_{kl} r^{n_{kl}} \exp(-\alpha_{kl} r^2)$ $(l = L)$ and $r^2[U^c{}_l(r) - U^c{}_L(r)] = \Sigma_k d_{kl} r^{n_{kl}} \exp(-\alpha_{kl} r^2)$ $(l < L)$.

(1) E. L. Muetterties, *Pure Appl. Chem.*, **54**, 83 (1982).
(2) G. A. Ozin, *Acc. Chem. Res.*, **10**, 287 (1977).
(3) H. F. Schaefer III, *Acc. Chem. Res.*, **10**, 287 (1977).
(4) S. P. Walch and W. A. Goddard III, *J. Am. Chem. Soc.*, **98**, 7908 (1976).
(5) K. Hermann and P. S. Bagus, *Phys. Rev. B: Solid State* **16**, 4195 (1977).
(6) A. B. Rives and R. F. Fenske, *J. Chem. Phys.*, **75**, 1293 (1981).
(7) P. S. Bagus and B. O. Roos, *J. Chem. Phys.*, **75**, 5961 (1981).
(8) B. H. Botch, T. Dunning, and J. F. Harrison, *J. Chem. Phys.*, **75**, 3466 (1981).
(9) C. W. Bauschlicher, S. P. Walch, and H. Patridge, *J. Chem. Phys.*, **76**, 1033 (1982).
(10) H. Basch, M. D. Newton, and J. W. Moskowitz, *J. Chem. Phys.*, **69**, 584 (1978).
(11) E. P. Kundig, D. McIntosh, M. Moskowitz, and G. A. Ozin, *J. Am. Chem. Soc.*, **95**, 7234 (1973).
(12) H. Basch and S. Topiol, *J. Chem. Phys.*, **71**, 802 (1979); **72**, 1422 (1980).

0002-7863/83/1505-3856$01.50/0

Table II. Valence Electron Basis Set for Platinum, Carbon, and Oxygen

atom	orbital	exponent	coeff
Pt	5d	19.78	−0.000 945 48
		2.095	0.375 287 7
		0.7435	0.718 747 3
	5d'	0.2257	1.0
	6s	0.9289	1.0
	6s'	0.1326	1.0
	6s''	0.04846	1.0
	6p	0.1500	1.0
	6p'	0.06000	1.0
C	2s	7.036	1.0
	2s'	0.4300	1.0
	2s''	0.1372	1.0
	2p	18.16	0.018 539 0
		3.986	0.115 436 0
		1.143	0.386 188 0
		0.3594	0.640 114 0
	2p'	0.1146	1.0
O	2s	13.59	1.0
	2s'	0.8572	1.0
	2s''	0.2653	1.0
	2p	35.18	0.018 237 3
		7.904	0.125 475 2
		2.305	0.392 222 1
		0.7171	0.629 322 8
	2p'	0.2137	1.0

ligand or metal–adsorbate systems.

We have, therefore, undertaken an ab initio RECP study of the lower energy electronic states of PtCO and have analyzed the resulting binding energy curve wave functions for the orbital interactions that dominate the bonding and determine the relative stabilities of the various states.

Calculational Details and Results

The RECP for the Pt atom and method of generation have been described previously[12,13] through $L = 3$. Morokuma and coworkers[14] have tested this Pt potential[12] on several square-planar metal complexes and found good agreement with experiment for geometry and metal–ligand bond lengths. Here we present the $L = 4$ component of the potential which should be the highest l value necessary.[15] The parameters of the potential are shown in Table I. The ECPs for the carbon and oxygen atoms were taken directly from Topiol et al.[16]

The fitted Pt atom basis set described previously[12] was reoptimized for the $5d^9 6s^1(^3D)$ state with little resultant change in the exponents. For the carbon and oxygen atoms a 3^s set was reoptimized for the respective atom electronic ground states by using the appropriate ECP[16] and Huzinaga's 5^p set[17] unchanged for the 2p orbitals. The resulting atom basis sets, including two sets of p functions for the 6p orbital of Pt, are shown in Table II.

The electronic configuration of composite Pt $5d^{10}(^1S)$ and ground state CO ($^1\Sigma^+$) fragments in a linear ($C_{\infty v}$) geometry can be written as

$$\text{Pt} \quad \pi_d^4\sigma_d^2\delta_d^4\sigma_s^0 \quad {}^1\Sigma^+$$

$$\text{CO} \quad n_O^2\sigma_{CO}^2 n_C^2\pi_{CO}^4\pi^*_{CO}{}^0\sigma_{CO}^{*0} \quad {}^1\Sigma^+$$

where the relevant empty orbitals have been deliberately included in order to define the internal set of molecular orbitals (MOs) for PtCO. The composite state is then $^1\Sigma^+$. For a Pt atom in its $5d^9 6s^1(^3D)$ ground-state configuration the d hole can be alternatively located in the σ_d, π_d, or δ_d orbitals to give the $^3\Sigma^+$, $^3\Pi$, and $^3\Delta$ electronic states, respectively. For example, when combined with $^1\Sigma^+$ CO

$$\text{Pt} \quad \sigma_d^2\pi_d^4\delta_d^3\sigma_s^1 \quad {}^3\Delta$$

gives the $^3\Delta$ composite PtCO state.

Multiconfiguration self-consistent field (MCSCF) and configuration interaction (CI) calculations were carried out on these four electronic states ($^1\Sigma^+$, $^3\Sigma^+$, $^3\Pi$, and $^3\Delta$) of linear PtCO by using the following procedure. For all these states the dominant CO bond correlating configurations [$\sigma_{CO}^2 \rightarrow \sigma^*_{CO}{}^2$, $\pi_{CO}^4 \rightarrow \pi_{CO}^2\pi^*_{CO}{}^2$ (closed shell only), and $\pi_{CO}^4 \rightarrow \pi^*_{CO}{}^4$] were included in the MC expansion in order to obtain a better description of the C=O bond and to generate a good set of CO antibonding orbitals for the CI. In addition, for the $^1\Sigma^+$ state the Pt $5d^{10}$ correlating configuration $5d^{10} \rightarrow 5d^8 6s^2(^1S)$ was added for the same reasons. Charge-transfer (CT) type configurations were purposely omitted from the MC expansions in order to attempt a separation of orbital and MC effects, in particular with regard to the relative σ dative (CO→Pt) and π-back-bonding (Pt→CO) interactions.

Each CI calculation included energy-selected single and double excitations from the dominant single configuration in the MC expansion, within the internal set of MOs defined above, plus single excitations into the 12 lowest (orbital) energy MOs from the

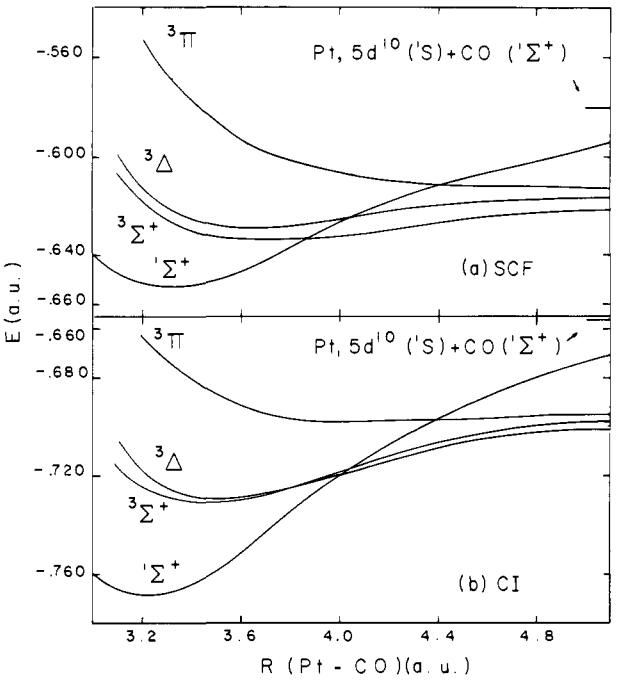

Figure 1. Binding energy curves for $^1\Sigma^+$, $^3\Sigma^+$, $^3\Delta$, and $^3\Pi$ states of PtCO. Energies are relative to −48 au.

Table III. Calculated Spectroscopic Constants for PtCO

	$^1\Sigma^+$	$^3\Sigma^+$	$^3\Delta$	$^3\Pi$
		MCSCF		
R_e, Å	1.732	1.943	1.942	
D_e, eV	1.99,[a] 0.92[b]	0.38[b]	0.30[b]	
k_e, au	0.188	0.096	0.089	
T_e, eV	0	0.52[c]	0.65[c]	2.34[b]
		CI		
R_e, Å	1.707	1.824	1.895	
D_e, eV	3.05,[a] 1.85[b]	0.84[b]	0.79[b]	
k_e, au	0.273	0.159	0.245	
T_e, eV	0	1.01[c]	1.06[c]	2.86[d]

[a] Relative to Pt $5d^{10}(^1S)$. [b] Relative to Pt $5d^9 6s^1$ (^3D). [c] Adiabatic. [d] Vertical.

(13) H. Basch, D. Cohen, and S. Topiol, *Isr. J. Chem.*, **19**, 233 (1980); H. Basch, *Symp. Faraday Soc.* **no. 14**, 149 (1980).
(14) K. Kitaura, S. Obara, and K. Morokuma, *Chem. Phys. Lett.*, **77**, 452 (1981).
(15) L. R. Kahn, P. Baybutt, and D. G. Truhlar, *J. Chem. Phys.*, **65**, 3826 (1976).
(16) S. Topiol, J. W. Moskowitz, and C. F. Melius, *J. Chem. Phys.*, **70**, 3008 (1979).
(17) S. Huzinaga, *J. Chem. Phys.*, **42**, 1293 (1965).

Table IV. Gross Overlap Populations for the Pt–C and C=O Bonds

	C=O[b]	PtCO[b,c]								PtCO[b,d]	
	$^1\Sigma^+$	$^3\Sigma^+$		$^1\Sigma^+$		$^3\Delta$		$^3\Pi$		$^1\Sigma^+$	
MO[a]	C=O	Pt–C	C=O	Pt–C	C=O	Pt–C	C=O	Pt–C	C=O	Pt–C	C=O
n_O	0.101	0.023	0.041	0.026	0.037	0.025	0.035	0.027	0.032	−0.027	0.001
σ_{CO}	0.555	−0.019	0.612	−0.004	0.611	−0.008	0.610	−0.012	0.609	−0.030	0.612
n_C	−0.307	0.384	−0.111	0.406	−0.078	0.419	−0.064	0.413	−0.056	0.252	−0.147
σ_d		0.104	−0.022	−0.035	−0.041	0.121	−0.047	0.088	−0.069	0.405	0.031
σ_s		0.013	−0.001	−0.240	−0.035	−0.297	−0.057	−0.359	−0.064	−0.044	−0.002
σ^*_{CO}	−0.013	−0.004	−0.013	−0.003	−0.014	−0.003	−0.014	−0.004	−0.014	−0.008	−0.013
π_{CO}	0.364	−0.034	0.360	−0.040	0.362	−0.038	0.365	−0.005	0.379	−0.070	0.346
π_d		0.147	−0.039	0.142	−0.028	0.132	−0.025	0.071	−0.029	0.210	0.027
π^*_{CO}	−0.003	−0.003	−0.002	−0.003	−0.003	−0.003	−0.003	−0.003	−0.004	−0.005	−0.001
total σ	0.336	0.476	0.506	0.150	0.480	0.256	0.463	0.153	0.438	0.548	0.482
total π_x	0.360	0.110	0.319	0.098	0.331	0.090	0.337	0.063	0.346	0.135	0.318
total	1.057	0.697	1.144	0.347	1.142	0.436	1.136	0.278	1.129	1.936	1.118

[a] Contributions are weighted by MCSCF occupancy. [b] C=O bond distance of 2.2 au. [c] Pt–C bond distance of 3.6 au. [d] Pt–C bond distance of 3.3 au.

Table V. Gross Orbital Populations for Pt, C, and O in PtCO[a]

		R = 3.1		R = 3.3		R = 3.6		R = 4.1		R = 5.1		R = 15.6	
atom	orbital	$^1\Sigma^+$	$^3\Delta$	$^1\Sigma^+$	$^3\Delta$	$^1\Sigma^+$	$^3\Delta$	$^1\Sigma^+$	$^3\Delta$	$^1\Sigma^+$	$^3\Delta$	$^1\Sigma^+$	$^3\Delta$
Pt	s	0.770	1.272	0.704	1.278	0.539	1.271	0.406	1.243	0.245	1.122	0.167	1.032
	p_σ	0.012	0.390	0.048	0.381	0.085	0.333	0.080	0.227	0.043	0.085	0	0
	p_π	0	0.021	0	0.020	0	0.016	0	0	0	0	0	0
	d_σ	1.426	1.501	1.507	1.560	1.614	1.626	1.701	1.702	1.803	1.860	1.916	1.968
	d_π	3.540	3.599	3.612	3.673	3.708	3.765	3.822	3.876	3.941	3.971	3.958	4.000
	d_δ	3.999	3.000	4.000	3.000	4.000	3.000	3.999	3.000	4.000	3.000	3.959	3.000
	charge	+0.250	+0.216	+0.125	+0.089	+0.053	−0.009	−0.009	−0.055	−0.031	−0.040	+0	+0
C	s	1.423	1.478	1.430	1.472	1.527	1.529	1.661	1.661	1.806	1.811	1.874	1.875
	p_σ	1.262	1.225	1.198	1.172	1.119	1.103	1.031	1.026	0.965	0.964	0.967	0.964
	p_π	1.408	1.405	1.355	1.349	1.282	1.281	1.193	1.190	1.086	1.092	1.036	1.046
	charge	−0.093	−0.107	+0.018	+0.007	+0.072	+0.087	+0.115	+0.122	+0.143	+0.133	+0.124	+0.115
O	s	1.807	1.809	1.804	1.807	1.801	1.805	1.803	1.807	1.815	1.814	1.808	1.808
	p_σ	1.316	1.325	1.323	1.330	1.330	1.333	1.332	1.334	1.340	1.344	1.352	1.353
	p_π	3.033	2.975	3.015	2.958	2.994	2.940	2.970	2.926	2.935	2.935	2.964	2.954
	charge	−0.156	−0.109	−0.143	−0.096	−0.125	−0.078	−0.106	−0.067	−0.113	−0.093	−0.124	−0.115

[a] Contributions are weighted by MCSCF occupancy. [b] Pt–CO distance (in au) at constant C=O bond length of 2.2 au.

corresponding MCSCF calculation. The number of resultant configurations was, typically, in the 200–500 range, depending on electronic state.

The MCSCF and CI calculations were carried out for a linear PtCO at varying Pt—C distances for a fixed C=O bond length of 2.20 au. The resultant energy curves are shown in Figure 1, and the calculated spectroscopic constants are displayed in Table III.

For the $^1\Sigma^+$ state more extensive MCSCF calculations were carried out by using a locally modified version of the ALIS[18] system of programs. The final MC expansion list included, besides the types of configurations enumerated above (including open-shell couplings for the $\pi_{CO}^4 \rightarrow \pi_{CO}^2\pi^*_{CO}^2$ excitations), simultaneous intrafragment single excitations ($\sigma_d \rightarrow \sigma_s$, $\pi_{CO} \rightarrow \pi^*_{CO}$), σ, π excitations on CO ($\sigma_{CO} \rightarrow \sigma^*_{CO}$, $\pi_{CO} \rightarrow \pi^*_{CO}$), and the dominant CT ($\pi_d^4 \rightarrow \pi_d^2\pi^*_{CO}^2$, closed- and open-shell couplings) configurations. The final MCSCF configuration list was determined by the iterative natural orbital analysis/valence CI feature of the ALIS system.[18] Optimization of the C=O bond distance in linear PtCO at fixed Pt—C bond lengths of 3.244 and 3.444 au gave the same equlibrium values of 2.19 au for the MCSCF and optimized C=O distances of 2.19 and 2.22 au, respectively, in the CI model. An analogous optimization of the free CO bond length gave an MCSCF equlibrium value of 2.19 au, although the CI value was 2.21 au. Thus in the $^1\Sigma^+$ state the equilibrium CO bond distance is only modestly affected, if at all, by bonding to a lone Pt atom.

In order to facilitate an interpretation of the orbital interactions involved in the Pt–CO bonding, Table IV contains details of the Mulliken gross overlap populations (GOP) in the various electronic states at different interfragment distances for the Pt—CO and PtC=O bonds. Gross atomic orbital populations by symmetry at a selected number of Pt—CO bond lengths is shown in Table V.

Discussion

Table III and Figure 1 show that $^1\Sigma^+$ is the lowest energy state with the largest binding energy and shortest interfragment equilibrium bond distance. Thus $^1\Sigma^+$ is calculated to be the electronic ground state. Next come the $^3\Sigma^+$ and $^3\Delta$ states with shallower binding energy curves and larger equilibrium Pt–CO bond distances. Finally, $^3\Pi$ is calculated to be dissociative. Actually, the CI results seem to indicate a very shallow (<0.05 eV) minimum for the $^3\Pi$ state at a relatively long (>2.0 Å) interfragment distance; but this result may already be beyond the resolution accuracy of these calculations. It should be noted that CI makes no changes in the relative orderings of the MCSCF calculated spectroscopic constant values. Also, the CI changes are all in the expected directions. Thus, the Pt–CO equilibrium bond distance (R_e) is shortened, the dissociation energy (D_e) increases, and the harmonic Pt–CO force constant (k_e) increases. The excitation energy (T_e) from the $^1\Sigma^+$ to the triplet states is also seen to increase uniformly, showing that CI preferentially stabilizes the $^1\Sigma^+$ state. In can thus be concluded that all the qualitatively important information about the Pt–CO bonding is already built in on the orbital MCSCF level.

The GOP for the C=O fragment alone (Table IV) shows the expected C=O bonding properties of n_O, σ_{CO} and π_{CO} and antibonding character of n_C, σ^*_{CO}, and π^*_{CO}. In passing to the PtCO complex as a function of decreasing Pt–CO distance n_O becomes less C=O bonding through increased localization on the oxygen atom and, correspondingly, n_C steadily loses a substantial part

(18) ALIS is described in K. Ruedenberg, L. M. Cheung, and S. T. Elbert, *Int. J. Quantun Chem.*, **16**, 1069 (1979).

of its C=O antibonding character through its bonding interaction with Pt. σ_{CO}, on the other hand, moderately increases in C=O bonding character and then decreases while π_{CO} uniformly decreases very slowly with shortening Pt—C bond length. In both these last cases the decrease in C=O bonding is due to increased interaction with the metal orbitals. π_d also contributes negatively to the C=O GOP due to mixing with the antibonding π^*_{CO} fragment orbital. Thus, the total GOP of the C=O bond shows a net increase value down to short Pt—CO bond distances mainly due to the loss of antibonding character in n_C which more than compensates for the decreased C=O π bonding. The total C=O GOP peaks in the 3.6–3.8-au Pt–CO distance range for all four states, where even at their calculated respective equlibrium Pt–CO bond lengths the C=O bond still has a slightly higher GOP value in the complex than in free CO.

This latter observation is reflected in the ALIS MCSCF and CI results for the $^1\Sigma^+$ state, referred to earlier, which show an increased value of the calculated C=O harmonic force constant in going from free C=O to PtC=O, although the equilibrium bond distances are calculated to stay essentially the same. Thus, with the reservation that overlap populations in metal complexes are not always consistent with known bonding characteristics,[19] the results obtained here point to a slightly strengthened C=O bond in PtC=O relative to free C=O. A stronger C=O bond would be expected to show an increased vibrational frequency for the C=O stretch mode in isolated PtCO. However, Kundig et al.[11] report ν_{CO} ~2052 cm^{-1} in low-temperature, matrix-isolated PtCO compared to the free CO value of ν_{CO} ~2143 cm^{-1}.[20] EELS studies of low exposure chemisorbed CO on Pt(111), where CO is assumed to be attached to a single Pt atom, show ν_{CO} ~2110 cm^{-1}.[21] Thus the experimental results generally show the CO vibrational frequency to shift to slightly lower values upon attachment to a metal atom. Possibly, this question demands a more detailed force field analysis,[22] encompassing all the atoms concerned, simultaneously. In any event, the results obtained here show that the coordinated C=O bond is stronger than might be expected from the experimental shifts in C=O frequency and that this increased strength is due to a balance between the σ- and π-bonding characteristics of the C=O bond.

The relationship between the decreased frequency of the C=O stretch mode upon complexation or chemisorption and the extent of Pt→CO back-donation (as reflected in the negative π_d contribution to the C=O GOP) has been discussed recently in relation to the alternative electrostatic model explanations of these frequency shifts.[23,24] The current calculations on PtCO (Table V) show that the charge on the Pt atom stays small and changes from negative to positive at R(Pt–CO) ≈ 3.6 ± 0.2 au for all four states, where the initially larger CO→Pt σ donation due to n_C is overtaken by the increasing Pt→CO π charge as the Pt–CO distance shortens. Thus, the electrostatic effect alone cannot explain the experimental vibrational frequency shifts, especially in light of the calculated near invariance of the C=O bond length with Pt–CO distance.

As displayed in Table IV the GOP for the Pt–CO bond shows a net bonding interaction for all four states in the general order $^1\Sigma^+ > {}^3\Delta > {}^3\Sigma^+ > {}^3\Pi$, although the $^3\Pi$ state is calculated to be not bound. We will therefore focus only on the qualitative contributory factors to this ordering in order to interpret the different binding energy curve characteristics shown in Figure 1. In the σ orbital manifold the most significant difference among the four states arises from the strongly antibonding behavior of σ_s which is empty in the single configuration description of the $^1\Sigma^+$ state. The absence of this long-range repulsive Pt(σ_s)–CO(n_C) interaction allows the CO to approach closer to the Pt and interact more strongly with its 5d orbital. Thus, comparing σ_d at 3.6 au (near the energy minimum for $^3\Delta$ and $^3\Sigma^+$) and 3.3 au (near the minimum for $^1\Sigma^+$) in Table IV for the $^1\Sigma^+$ state shows the enhanced bonding character of σ_d at the shorter distance.

A similar effect is observed in the π levels where the π_d GOP is enhanced by the increased Pt($5d_\pi$)–CO(π^*_{CO}) interaction as the Pt–C distance decreases. This interaction, of course, gives rise to the famous Pt→CO π-back-bonding effect which is thus larger in the $^1\Sigma^+$ state compared to the other states. However, the $^3\Pi$ state, with only ~$^3/_4$ the contribution of this bonding interaction, due to the fractional occupany of the π_d orbital, has a weaker Pt–CO π-bonding interaction. It thus appears that the π-bonding interaction is an important, if not dominant, effect in determining the relative stabilities among the PtCO electronic states.

The gross atomic orbital populations in Table IV offer some interesting insights into the Pt–CO interactions and the orbital configurations of the fragments. The increasingly dominating role of the Pt($5d_\pi$) → CO($2p_\pi$) charge transfer over CO_σ → Pt_σ with decreasing Pt–CO distance (R) is clearly seen in the populations and has already been noted. The oxygen atom populations are relatively stable, but the carbon atom shows a substantial shift of population from its 2s to $2p_\sigma$ orbital as R decreases, apparently to enhance the Pt–C interaction in the n_C and σ_d MOs. the Pt atom 6s orbital population is substantially larger for both the $^1\Sigma^+$ and $^3\Delta$ states near their appropriate R_e values than would be expected from their $5d^{10}$ and $5d^96s^1$ dissociation limit atom configurations, respectively. The $^1\Sigma^+$ state at R = 3.3 au (1.746 Å), for example, has a Pt atom configuration that is much closer to $5d^96s^1$ than to $5d^{10}$. Analogously, the 5d orbital population in the $^3\Delta$ state at R = 3.6 au (1.905 Å) is only 8.39 e, and this includes contributions from the $x^2 + y^2 + z^2$ combinations of the d-type basis functions. On the other hand, the $^3\Sigma^+$ state at that distance has closer to 9 d-type e. Thus, the $5d^86s^2(^3F)$ configuration must play an important role in the $^3\Delta$ state, as suggested by Walch and Goddard for NiCO,[4] and the $5d^96s^1(^1D)$ state probably contributes strongly to the $^1\Sigma^+$ ground state of PtCO.[25]

A comparison of these results on PtCO with previous studies on NiCO[4-7] shows a parallel with the work of Rives and Fenske,[6] who were, apparently, the first to find the $^1\Sigma^+$ state below $^3\Delta$, $^3\Sigma^+$, and $^3\Pi$ in NiCO.[26] Two differences between PtCO and NiCO are worth noting. In the NiCO system diffuse d orbitals and extensive CI were required to obtain bound triplet states. In PtCO single configuration (with respect to mixed Pt–CO correlation) SCF calculations using an atomic valence Pt orbital basis are sufficient to obtain both $^3\Delta$ and $^3\Sigma^+$ bound. The CI calculations just quantitatively enhance the trends already clearly observable in the SCF results. These differences between PtCO and NiCO[6] partially reflect the better single configuration description of the Pt atom ^3D, ^3F, and ^1S multiplet energy separations using the Pt atom relativistic ECP[12] compared to atomic nickel. Probably, part of the difference also lies in the intrinsically stronger bonding of CO to Pt relative to Ni in the bare systems. Muetterties et al.[27] note that both homonuclear and polynuclear metal–CO bond energies generally increase in going down the transition-metal series. A similar trend is found in CO–metal surface bond strengths.

Two more aspects are worth noting. The first is the effect of spin–orbit interaction on the energy levels of PtCO. Spin–orbit coupling as a first-order perturbation will lower the energy of the $^2\Delta_{5/2}$ state by an amount λ, the spin–orbit coupling constant, which in Pt^+ is λ ~0.4 eV.[11] Since both the SCF and CI results give an adiabatic $^1\Sigma^+ - {}^3\Delta$ splitting that is larger than this value, the spin–orbit coupling term will not reverse the calculated ordering

(19) J. H. Ammeter, H. B. Burgi, J. C. Thibeault, and R. Hoffmann, *J. Am. Chem. Soc.*, **100**, 3686 (1978).
(20) K. P. Huber and G. Herzberg, "Constants of Diatomic Molecules", Van Nostrand Reinhold Co., New York, 1979.
(21) A. M. Baro and H. Ibach, *J. Chem. Phys.*, **71**, 4812 (1979).
(22) T. Wentink, Jr., *J. Chem. Phys.*, **30**, 195 (1959).
(23) N. S. Hush and M. L. Williams, *J. Mol. Spectrosc.*, **50**, 349 (1974).
(24) J. W. Davenport, *Chem. Phys. Lett.*, **77**, 45 (1981).
(25) A reviewer has suggested the role of the ^1D state based on comments by W. A. Goddard and C. W. Bauschlicher about the corresponding $^1\Sigma^+$ state of NiCO.
(26) D. T. Clark, B. J. Cromarty, and A. Sgamelloti, *Chem. Phys. Lett.*, **55**, 482 (1978) found $^3\Delta$ below $^1\Sigma^+$ in NiCO.
(27) E. L. Muetterties, T. N. Rhodin, E. Band, C. F. Brucker, and W. R. Pretzer, *Chem. Rev.*, **79**, 91 (1979).

of these two states. The second point concerns a possibly nonlinear PtCO. We find both the SCF $^1\Sigma^+$ and $^3\Sigma^+$ states to be strongly linear. Clark et al.[26] found the $^3\Delta$ state in NiCO to be weakly bent, and the same behavior is expected also for $^3\Delta$ in PtCO. Therefore, bending PtCO is not expected to change the ordering of electronic states found for the linear geometric configuration.

Acknowledgment. We wish to thank Dr. S. T. Elbert for supplying us with his latest version of ALIS. This work has been supported by the Israel Commission for Basic Research, Jerusalem, Israel. We acknowledge very useful comments by the reviewers.

Registry No. PtCO, 49819-49-0.

Electronic Structure of Alkylated Imidazoles and Electronic Spectra of Tetrakis(imidazole)copper(II) Complexes. Molecular Structure of Tetrakis(1,4,5-trimethylimidazole)copper(II) Diperchlorate

Ernest Bernarducci, Parimal K. Bharadwaj, Karsten Krogh-Jespersen,* Joseph A. Potenza,* and Harvey J. Schugar*

Contribution from the Department of Chemistry, Rutgers, The State University of New Jersey, New Brunswick, New Jersey 08903. *Received September 7, 1982*

Abstract: The synthesis, crystal structure, electronic spectra, and ESR spectra are reported for the title complex (**1**). This complex crystallized as orange-brown plates in the orthorhombic space group *Pccn* with a = 13.65 (1) Å, b = 13.90 (1) Å, and c = 17.54 (1) Å, d_{obsd} = 1.40 (1) g/cm^3, d_{calcd} = 1.403 g/cm^3, and Z = 4. Least-squares refinement of 1346 reflections having $F^2 \geq 3\sigma$ gave a conventional R factor of 0.063 and R_{wF} = 0.060. The structure consists of discrete tetrakis(1,4,5-trimethylimidazole)copper(II) cations with point symmetry $\bar{1}$ whose planar CuN_4 units exhibit Cu-N distances of 2.004 (7) and 1.995 (7) Å and N-Cu-N angles of 89.5 (3) and 90.5 (3)°. Dihedral angles between the imidazole and CuN_4 planes are 75.7 and 75.5°. Energies of the molecular orbitals and electronically excited states of imidazole and of several methylated imidazoles have been calculated by an INDO/S method. The observed ligand $\pi \rightarrow \pi^*$ and n,π_1,π_2(ligand) $\rightarrow$ Cu(II) ligand to metal charge-transfer (LMCT) absorptions of the title complex and other Cu(II)-imidazole complexes are discussed and compared. Preliminary LMCT spectra are presented for the yellow diamagnetic tetrakis(1,2-dimethylimidazole)nickel(II) diperchlorate complex and its Cu(II) analogue. An experimental justification for assigning the charge-transfer absorptions as LMCT instead of MLCT is presented.

The presence of Cu(II)-imidazole bonding in proteins has been demonstrated crystallographically for plastocyanin,[1] azurin,[2] and superoxide dismutase[3] and has been inferred for stellacyanin,[4] serum albumin,[5] galactose oxidase,[6] cytochrome *c* oxidase,[7] ceruloplasmin,[8] hemocyanins,[9] and tyrosinases.[10] The wide biochemical scope of Cu(II)-imidazole bonding has prompted numerous spectroscopic studies of low molecular weight Cu(II) chromophores including ligation from imidazoles,histidine, histamine, and histidine-containing peptides. Tetragonal Cu(II) chromophores of these types exhibit four or five absorption maxima in the 29 000-45 000-cm^{-1} spectral region, including a weak near-UV band or shoulder ($\epsilon \sim 300$) thought to arise from π(imidazole) $\rightarrow$ Cu(II) ligand to metal charge-transfer (LMCT).[9,11,12] We have chosen to elaborate the nature of imidazole $\rightarrow$ Cu(II) LMCT absorptions exhibited by well-defined model Cu(II) complexes to help facilitate the assignment of corresponding absorptions in the spectra of various Cu(II) protein chromophores. These studies have yielded several useful results.[13,14] First, Cu(II)-imidazole chromophores exhibit three types of LMCT absorptions that originate from the sp^2 nitrogen lone pair (n) and from two π-symmetry ring orbitals, one (HOMO, π_1) with mostly carbon character and the other (π_2) with substantial nitrogen character. Tetragonal Cu(II)-imidazole complexes exhibit overlapping n(imidazole) $\rightarrow$ Cu(II) LMCT and ligand $\pi \rightarrow \pi^*$ absorptions at $\sim$45 000 cm^{-1}; the π_2(imidazole) $\rightarrow$ Cu(II) and π_1(imidazole) $\rightarrow$ Cu(II) LMCT absorptions occur at approximately 35 000 and 30 000 cm^{-1}, respectively. Corresponding π(imidazole) $\rightarrow$ Cu(II) LMCT absorptions have been noted in the UV spectra of native and two types of Cu(II)-doped superoxide dismutase.[15] Second, owing to the small ligand fields[16]

(1) Coleman, P. M.; Freeman, H. C.; Guss, J. M.; Murata, M.; Norris, V. A.; Ramshaw, J. A. M.; Venkatappa, M. P. *Nature (London)* **1980**, *272*, 319-24.
(2) Adman, E. T.; Stienkamp, R. E.; Sieker, L. C.; Jensen, L. H. *J. Mol. Biol.* **1978**, *123*, 35-47.
(3) Richardson, J. E.; Thomas, K. A.; Rubin, B. H.; Richardson, D. C. *Proc. Natl. Acad. Sci. U.S.A.* **1975**, *72*, 1349-52.
(4) Ulrich, E. L.; Markley, J. L. *Coord. Chem. Rev.* **1978**, *27*, 109-40.
(5) Bradshaw, R. A.; Shearer, W. T.; Gurd, F. R. N. *J. Biol. Chem.* **1968**, *243*, 3817-25.
(6) Bereman, R. D.; Kosman, D. J. *J. Am. Chem. Soc.* **1977**, *99*, 7322-25.
(7) Palmer, G.; Babcock, G. T.; Vickery, L. E. *Proc. Natl. Acad. Sci. U.S.A.* **1976**, *73*, 2206-10.
(8) Fee, J. A. *Struct. Bonding (Berlin)* **1975**, *23*, 1-60.
(9) Freedman, T. B.; Loehr, J. S.; Loehr, T. M. *J. Am. Chem. Soc.* **1976**, *98*, 2809-15.
(10) Himmelwright, R. S.; Eickman, N. C.; LuBien, C. D.; Lerch, K.; Solomon, E. I. *J. Am. Chem. Soc.* **1980**, *102*, 7339-44.
(11) Bryce, G. F.; Gurd, F. R. N. *J. Biol. Chem.* **1966**, *241*, 122-29.
(12) Amundsen, A. R.; Whelan, J.; Bosnich, B. *J. Am. Chem. Soc.* **1977**, *99*, 6730-39.
(13) Fawcett, T. G.; Bernarducci, E.; Krogh-Jespersen, K.; Schugar, H. J. *J. Am. Chem. Soc.* **1980**, *102*, 2598-2604.
(14) Bernarducci, E.; Schwindinger, W. F.; Hughey, J. L., IV; Krogh-Jespersen, K.; Schugar, H. J. *J. Am. Chem. Soc.* **1981**, *103*, 1686-91.
(15) Pantoliano, M. W.; Valentine, J. S.; Nafie, L. A. *J. Am. Chem. Soc.* **1982**, *104*, 6310-17.
(16) Solomon, E. I.; Hare, J. W.; Dooley, D. M.; Dawson, J. H.; Stephens, P. J.; Gray, H. B. *J. Am. Chem. Soc.* **1980**, *102*, 168-78.

0002-7863/83/1505-3860$01.50/0